Hindawi
Advances in Civil Engineering
Volume 2020, Article ID 8894138, 14 pages
https://doi.org/10.1155/2020/8894138

Research Article

Numerical Analysis on the Performance of the Underwater Excavation

Bo Li[1], **Cangqin Jia**[1], **Guihe Wang**[1], **Jun Ren**[2], **Gaofeng Lu**[3] and **Nannan Liu**[4]

[1]*School of Engineering and Technology, China University of Geosciences (Beijing), Haidian District, Beijing 100083, China*
[2]*CCCC Tunnel Engineering Company Limited, Chaoyang District, Beijing 100102, China*
[3]*Beijing Metro Construction Administration Corporation Ltd, Fengtai District, Beijing 100068, China*
[4]*School of Energy Resources, China University of Geosciences (Beijing), Haidian District, Beijing 100083, China*

Correspondence should be addressed to Cangqin Jia; jiacangqin@cugb.edu.cn

Received 19 June 2020; Revised 28 September 2020; Accepted 19 October 2020; Published 10 November 2020

Academic Editor: Chunshun Zhang

Based on the Yongdingmen Station of Beijing Metro, the underwater excavation method for deep foundation pit was introduced. This study constructed a numerical analysis model to analyze the performance of surface settlement and lateral wall deflection in the process of underwater excavation. Results showed that this method was better to control the surface settlement and lateral wall deflection compared with other dewatering excavations. In detail, most of the surface settlement was caused during the dry excavation stage and dewatering excavation stage while the deflection caused by underwater excavation only accounted for about 10% of the total settlement. Besides, the maximum settlement occurred 0.25~0.5 H_e behind the retaining wall and the value was 0.04% H_e. Similar to the result of the surface settlement, most of the lateral wall deflection had been completed before the underwater excavation, which only caused about 7% of the total deflection. The maximum wall deflection and its location were approximately 0.06% H_e and 0.5 H_e, respectively. Moreover, a series of 3D numerical analyses were studied on the design parameters of the underwater excavation method. This study can be used as a reference for general performance and structural design of foundation pits with underwater excavation.

1. Introduction

The excavation of the foundation pit was often accompanied by structural deflection [1] and surface settlement [2, 3]. Among the causes of large deflection, groundwater was a common problem that directly determines the selection of excavation technology and retaining structure. To avoid the engineering disaster caused by the large deflection, it was necessary to adopt effective groundwater control measures and reliable water-stop structures [4, 5]. According to the research, there were three methods to control the groundwater in the excavation process: first, setting multiple dewatering wells to control the groundwater level at a certain height before excavation, which was suitable for the excavation with small depth and low moisture content [6–8]; second, employing a water curtain to cut off the underground water directly, which generally requires the structure to have a large embedded depth. [9–11]; third, combining the water interception and grouting reinforcement treatment, which requires proven technology and engineering cost [5, 12].

Influenced by the existing metro lines, the increase of excavation depth of the Beijing subway station will cause most or even all of the station structure to enter the confined water layer. Blindly using traditional dewatering excavation will bring multiple problems such as water resource loss and high cost of precipitation. On this basis, a new excavation method of underwater excavation has appeared in some engineering. Almaleh et al. [13] introduced the basic expansion project of the Crystal River with underwater excavation and underwater grouting. Archontidou-Argyri et al. [14] used the method of underwater excavation to mine cultural relics, which achieved the effect of controlling ground deflection. Hu [15] proposed the underwater excavation to balance the external water pressure and passive

Earth pressure by using the recharge water in the Meizizhou air shaft project. Qu et al. [16] applied the nondrainage excavation method in an excavation of Shanghai to control the ground settlement.

It can be seen from the above excavations that this method can effectively protect groundwater resources and control soil deformation. However, due to the particularity of underwater excavation, the successful cases were limited. Most of the literature still focused on the summary of construction technology and there was no further study on the deformation characteristics and the structural design for this new excavation method. Based on a new well-documented excavation project of Yongdingmen station abbreviated as the YDM station, this paper established an underwater excavation model, in which a series of 3D finite element analyses were carried out to investigate the performance and mechanism of the underwater excavation combined with the field observation.

2. Project Overview

2.1. Project Background. Figure 1 shows the stratigraphic section of the YDM station studied in this article. The soil layer above the water level was mainly alternating silt sand (SM) and silty clay layers (CL), and below the water level was a huge thickness of pebble stratum (Cb). The excavation bottom was located in the pebble stratum filled with water and large-diameter pebbles. The pebble diameter greater than 20 mm was 50%~80% and often mixed with pebbles and boulders, which has a maximum diameter of 80 mm. Therefore, the YDM excavation was unsuitable for traditional dewatering excavation due to the high permeability and large water inflow at the excavation bottom. Furthermore, there was no thickness bearing Earth layer below the excavation bottom. If the water outside the pit was cut off directly, a diaphragm wall with a depth of 60 m was required, which will increase the project difficulty and cost waste. To solve the above construction problems and protect the groundwater resources in Beijing, the underwater excavation method was proposed for YDM excavation.

Figure 2 shows the top view of the geometric parameters of the YDM project and the layout of the deflection monitoring points. The diaphragm wall with 1.2 m thick was used as the retaining wall of the excavation, on which 12 inclinometers were installed at different locations. Several 1 m thick cross walls divided the foundation pit into 16 bays.

Figure 3 shows the schematic graph of retaining structure, stratum, and excavation (section A-A), which was finished in eight steps using the traditional excavation method combined with the underwater excavation method. The cross walls were backfilled within concrete between GL-32 m and GL-44 m (GL referred to the ground surface level). The concrete slabs 1BF, 2BF, and 3BF were the beam-floor systems, 4.5 m in spacing for 1BF, and 9 m in spacing for 2BF, respectively. A 4-meter-thick underwater concrete bottom seal was performed. The construction depth was 36.5 m, and the groundwater level was GL-19.0 m. The toes of diaphragm walls and cross walls were embedded 8 m in the Cb layer. The critical steps of the YDM project are shown in Figure 4.

2.2. Establishment of the Finite Element Model. Figure 5 illustrates the YDM project excavation and three-dimensional finite element mesh used for analysis. A 10-noded tetrahedral element was applied to simulate the soil volume. Soil movements normal to the four vertical sides were restrained (roller boundary), whereas soil movements were restrained in all directions at the bottom of the geometry (fixed boundary) [17]. The distance between the diaphragm walls and the outer boundary of the mesh was larger than five times the final excavation depth (He) to minimize the boundary effect.

The hardening soil model [18], abbreviated as HS model, was adopted for this study. This model must input 11 parameters $(c', \varnothing', \psi, E_{50}^{\text{ref}}, E_{\text{oed}}^{\text{ref}}, E_{\text{ur}}^{\text{ref}}, m, \nu_{\text{ur}}, p^{\text{ref}}, K_o^{\text{NC}}, R_f)$ to reflect the mechanical behavior of soil. Table 1 lists the physical meaning and estimation method of various parameters. These parameters can be solved according to the formula in the table through the basic physical parameters obtained from the survey data. For the silt soil layer, the unloading/reloading referential stiffness $(E_{\text{ur}}^{\text{ref}})$ can be obtained by the initial void ratio (e) and the swelling index (Cs), and then $(E_{50}^{\text{ref}})$and $(E_{\text{oed}}^{\text{ref}})$ can be calculated. For the sandy soil layer, then $(E_{\text{oed}}^{\text{ref}})$ and $(E_{\text{ur}}^{\text{ref}})$ should be calculated followed by (E_{50}^{ref}) which was calculated by the elastic modulus E_S according to the evaluation in Table 1.

The structural members such as diaphragm walls, cross walls, and concrete slabs employed were made of plate elements and simulated as linear elastic material as well as the concrete strut. Also, the interface friction angle between the structure and the soil was the same as that of the soil, and the mechanical behavior of the contact interface was set according to the Mohr–Coulomb criterion. Considering the possibility of the microcracks in concrete after structural deflection, the elastic modulus of the structure has been reduced by 20% [26,27]. The input parameters of the soil layer and structure are all shown in Table 2.

3. Monitoring Results and Discussion

3.1. Ground Surface Settlement. The settlement of 3D-analysis in 8 excavation stages is extracted in Figure 6. The results show that, along with the Earth excavation, the value and the influential range of the soil settlement gradually increased. The main increase in settlement occurred before the underwater excavation (step 6). During the underwater excavation stage, the surface settlement increased slowly. Besides, the surface settlement in step 4 was obviously increased due to the strong Earth permeability of GL-22 to GL-28.

Figure 7 showed the 3D-analysis results and field observations of surface settlement (δ_v) at different distances (d) from the middle line of the diaphragm wall. The 3D-analysis results were fit well with the field observations under various steps. The error of two analysis results was approximately 1~2 mm, which was an allowable error range of projects. However, because the excavations equipment used for underwater excavation and underwater concrete filling were placed at the edge of the excavation for a long time, the result of the observation was slightly larger than the 3D-

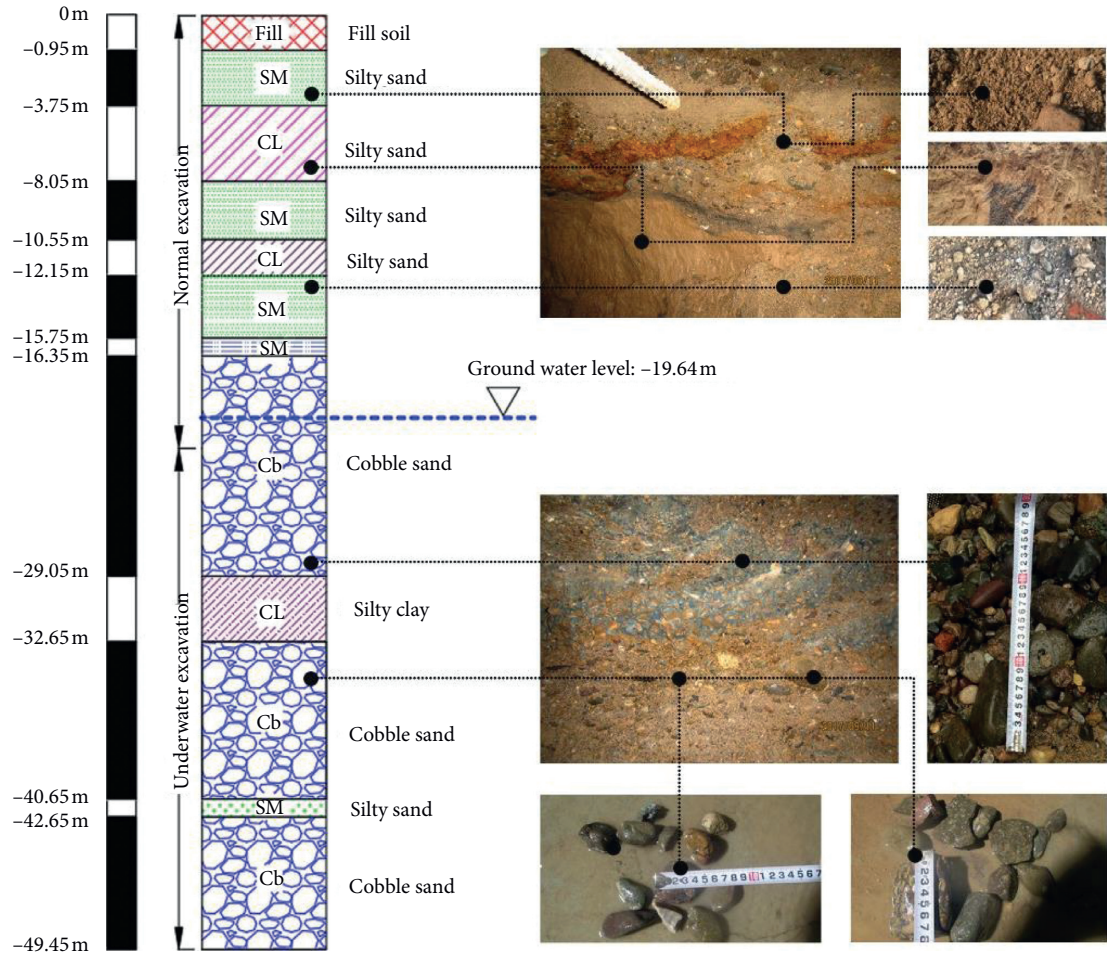

Figure 1: Stratigraphic profile of YDM excavation.

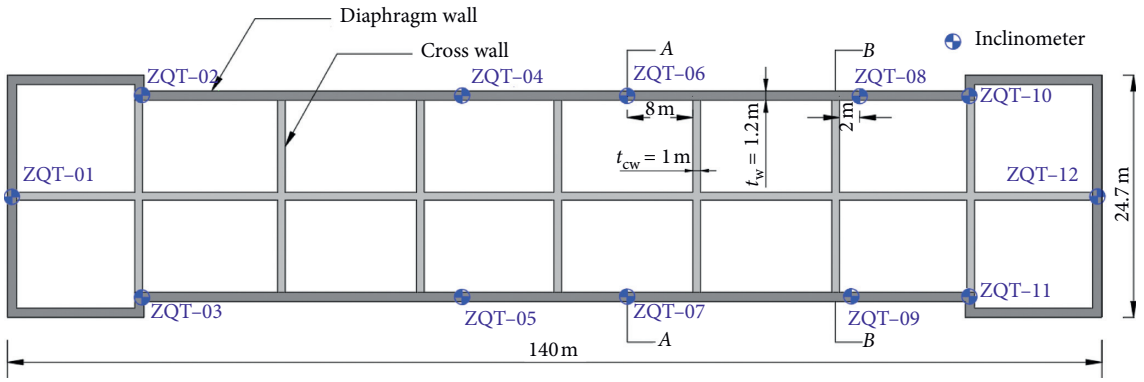

Figure 2: Geometric plane of retaining wall and monitoring layout.

analysis result within 10 m from the edge of the excavation and decreased faster beyond 10 m away from the excavation.

As shown in Figure 7, most of the settlement occurred between step 1 and step 4. The δ_v of 3D-analysis and observations were 12.4 mm and 13.2 mm, which had already accounted for 86.7% and 81.9% of the final settlement (14.3 mm and 16.1 mm), respectively. During the underwater excavation (step 6), the δ_v of 3D-analysis and observation were increased by 1.3 mm and 1.6 mm, which only accounted for 9% and 10% of the final settlement. This increment was far less than the increased δ_v of 2.8 mm and 3.1 mm in the drainage excavation (step 4) under the condition of little difference in excavation depth. To better explain the surface settlement characteristics during underwater excavation, the research results of Hsieh [28] and this study are plotted in Figure 8. The settlement influence area in the figure

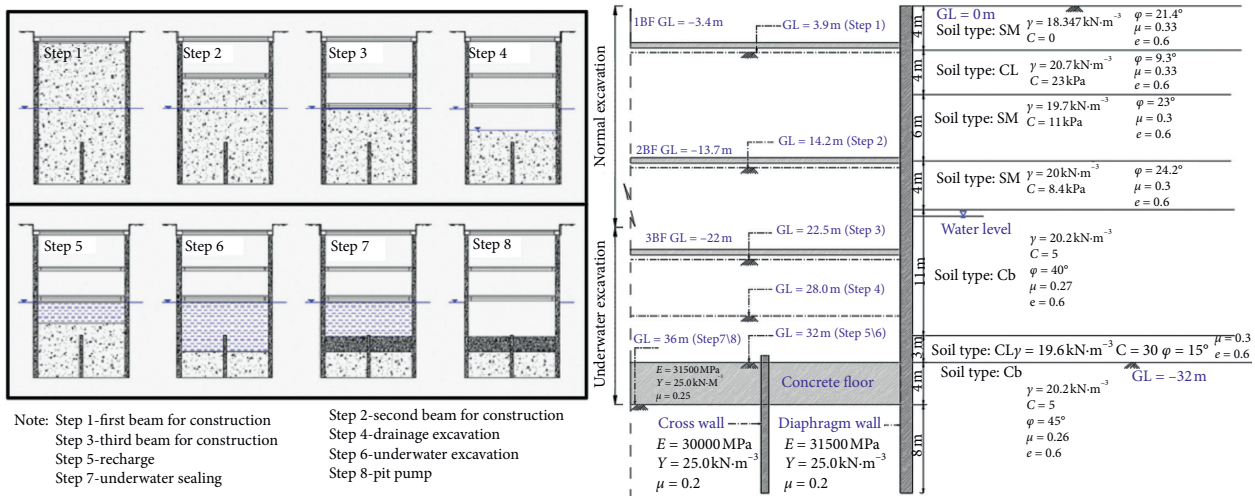

Figure 3: Excavation geometry and stratigraphy for YDM project.

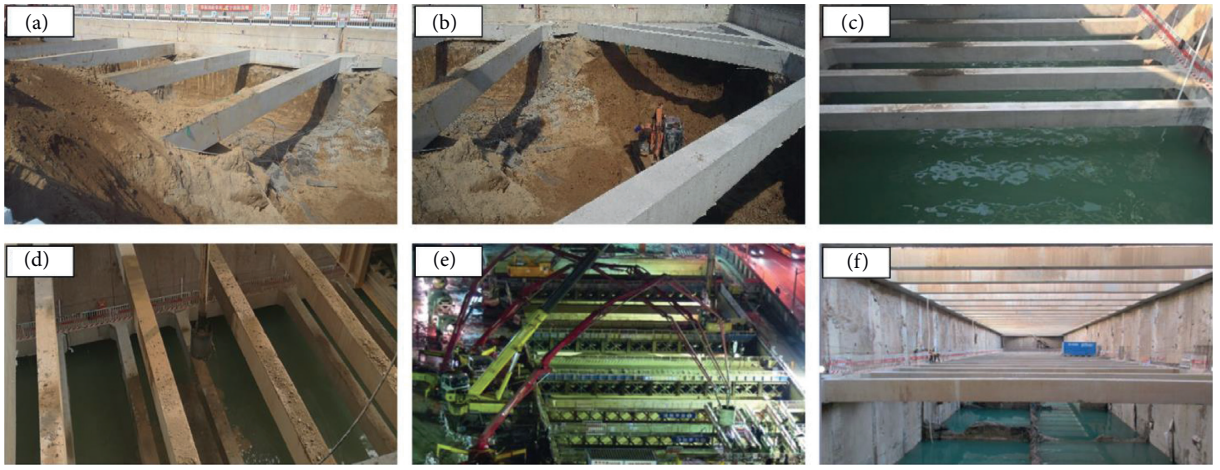

Figure 4: Critical steps during excavation for YDM project. (a) Step 1, (b) step 4, (c) step 5, (d) step 6, (e) step 7, and (f) step 8.

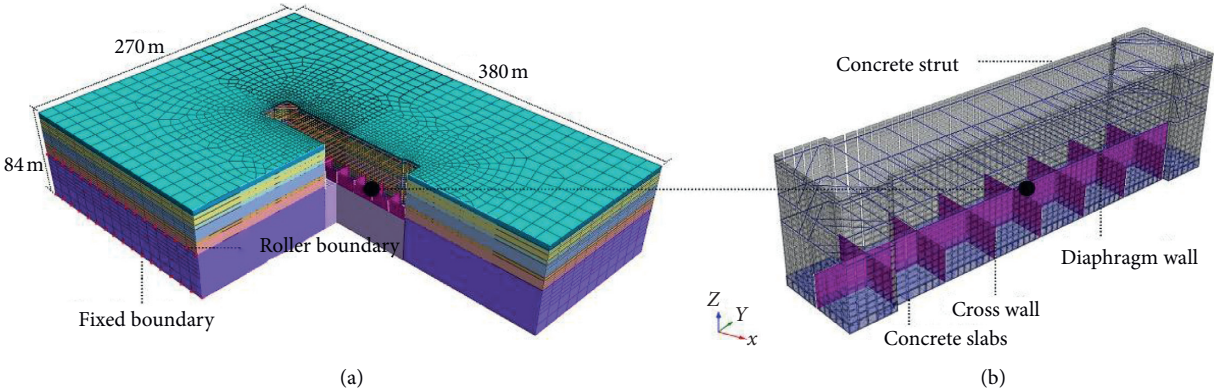

Figure 5: Three-dimensional finite element mesh for analysis.

was represented by the ratio of d and the excavation depth H_e and the ratio of δ_v and the maximum settlement δ_{vm}.

The settlement profile presented a groove type, and the settlement area can be divided into two parts. The main settlement area was $(\delta_v/\delta_{vm}) \geq 0.1$and the secondary settlement area was $(\delta_v/\delta_{vm}) \geq 0.1$. Hsieh showed that the main settlement area was within $(d/H_e) = 2$ while the secondary settlement area was between $(d/H_e) = 2$ and $(d/H_e) = 4$. Besides, the

Table 1: Parameters of the HS model.

Symbol	Physical implication	Method of evaluation	References
ψ	The angle of dilatancy	$\psi = \phi - 30^{\circ}$ $(\phi > 30^{\circ})$ $\psi = 0$ $(\phi < 30^{\circ})$	Bolton [19]
E_{50}^{ref}	Modulus of elasticity under partial loading	$E_{50}^{\text{ref}} = (E_{ur}^{\text{ref}}/3)$ for clay $E_{50}^{\text{ref}} = (E_S/3(\sigma'/p^{\text{ref}*})^m)$ for sand	Calvello and Finno [20] Khoiri and Ou [21]
$E_{\text{oed}}^{\text{ref}}$	Modulus of elasticity of in compression test	$E_{\text{oed}}^{\text{ref}} = 0.7E_{50}^{\text{ref}}$ for clay $E_{\text{oed}}^{\text{ref}} = 1.5E_{50}^{\text{ref}}$ for sand	Calvello and Finno [20] Khoiri and Ou [21]
$E_{\text{ur}}^{\text{ref}}$	The referential unloading/reloading stiffness	$E_{\text{ur}}^{\text{ref}} = ((3(1+e)p^{\text{ref}}(1-2)\nu_{\text{ur}})/(c_s/\ln 10))$ for clay $E_{\text{ur}}^{\text{ref}} = 3E_{50}^{\text{ref}}$ for clay	Lim et al. [22] Khoiri and Ou [21]
m	Power index of the stress level of stiffness	$m = 1.0$ for clay $m = 0.5$ for sand	Schanz et al. [23]
R_f	Strength failure ratio	0.9	Duncan and Chang [24] Schanz et al. [23]
ν_{ur}	Poisson's ratio in the unloading-reloading state	0.2	—
K_0^{NC}	K_0 value for normal consolidation	$1 - \sin \varnothing$	Jaky [25]

*The referential pressure $p^{\text{ref}} = 100$ kPa.

Table 2: Input parameters of the soil layer and structural members for the YDM excavation.

Soil	μ	c_s(kPa)	K_0^{NC}	E_{50}^{ref}(MPa)	$E_{\text{oed}}^{\text{ref}}$(MPa)	$E_{\text{ur}}^{\text{ref}}$(MPa)	R_f	m	(φ/°)	(ψ/°)
SM	0.33	0	0.64	18.347	18.347	55.041	0.9	0.5	21.4	0
CL	0.33	23	0.84	22.439	22.439	67.317	0.9	1.0	9.3	0
SM	0.3	11	0.61	23.009	23.009	69.297	0.9	0.5	23.0	0
SM	0.3	8	0.59	31.218	31.218	63.645	0.9	1.0	24.2	0
CB	0.27	5	0.35	132	132	396	0.9	1.0	40.0	10
CL	0.3	30	0.74	32.076	32.076	96.228	0.9	0.5	15.0	0
CB	0.26	5	0.29	198	198	594	0.9	1.0	45.0	15

Structure type	Thickness(m)	E(MPa)	(γ/kN · m^{-3})	μ
Diaphragm wall	1.2	25200*	25	0.15
Cross wall	1.0	25200*	25	0.15
Concrete slabs	4.0	23100*	24	0.3
Concrete strut	1.0	6200*	25	0.15

*Young's modulus was reduced by 20%.

maximum settlement δ_{vm} was at the ratio of $(d/H_e) = 0.5$ and δ_v close to the wall was 0.5 times of δ_{vm}. In this study, however, the main settlement area was within $(d/H_e) = 1$ while the secondary settlement area was little. The maximum settlement $(\delta_v/\delta_{\text{vm}}) = 1$ was at the ratio of $(d/H_e) = 0.25 \sim 0.5$, and δ_v close to the wall was 0.25 times of δ_{vm}.

Kun [29] and Xu [30] counted the maximum settlement distribution of excavations with traditional dredging excavation, as shown in Figure 9. The measured data indicated that δ_{vm} was distributed between 0.1% He and 1.0% He, which was far larger than that of the YDM project (0.04% He on average). The above analysis further proved that the underwater excavation method had better resistance to the surface settlement; that is, the settlement influence range and the maximum settlement were much small than the predicted value compared with the traditional dredging excavation.

3.2. Lateral Wall Deflection. Figure 10 shows the wall deflection of the 3D-analysis at 8 construction steps. The results showed that the wall deflection increased with Earth excavation but rapidly decreased around the position of the cross wall. Most of the lateral wall deflection occurred before drainage excavation (step 4). During the whole process of underwater excavation, the wall deflection was only slightly increased in the area between adjacent cross walls, and the maximum deflection position was no longer moving towards the excavation bottom.

Figure 11 shows the 3D-analysis results and field observations of surface settlement (δ_h) at the midline of the diaphragm wall on the long side. There was an error of 3~4 mm between the observations and the 3D-analysis results. The reason was that, in step 2, the excavation depth was up to 10 m and the free face of the diaphragm wall was unsupported for a long time, as well as the mechanical load and construction disturbance. Moreover, the water level in the pit did not recharge to a certain height for the first time in the practical excavation, for which δ_h of the observations increased below the third beam compared with those of the 3D-analysis. Although the error existed, the deformation trend and the deformation increment of two results in each step were similar.

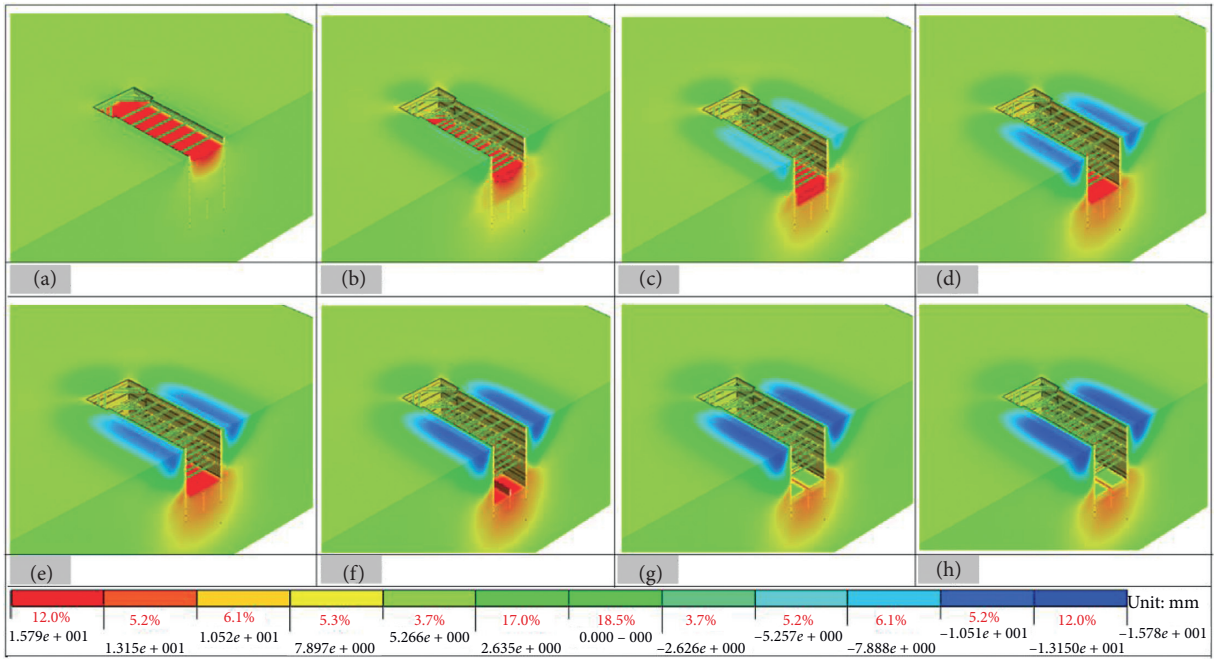

Figure 6: The contour of settlement with 3D-analysis for YDM project. (a) Step 1, (b) step 2, (c) step 3, (d) step 4, (e) step 5, (f) step 6, (g) step 7, and (h) step 8.

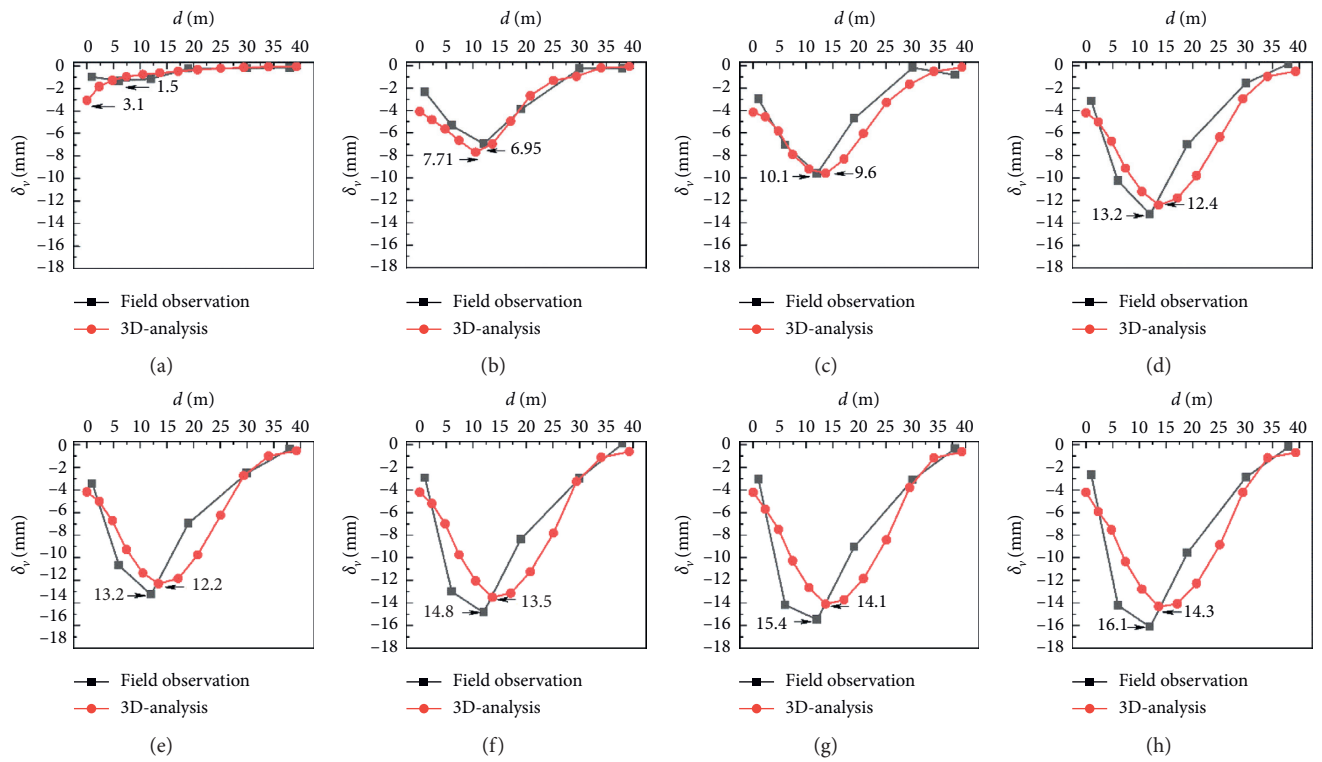

Figure 7: Surface settlement curve under various working conditions for YDM project. (a) Step 1, (b) step 2, (c) step 3, (d) step 4, (e) step 5, (f) step 6, (g) step 7, and (h) step 8.

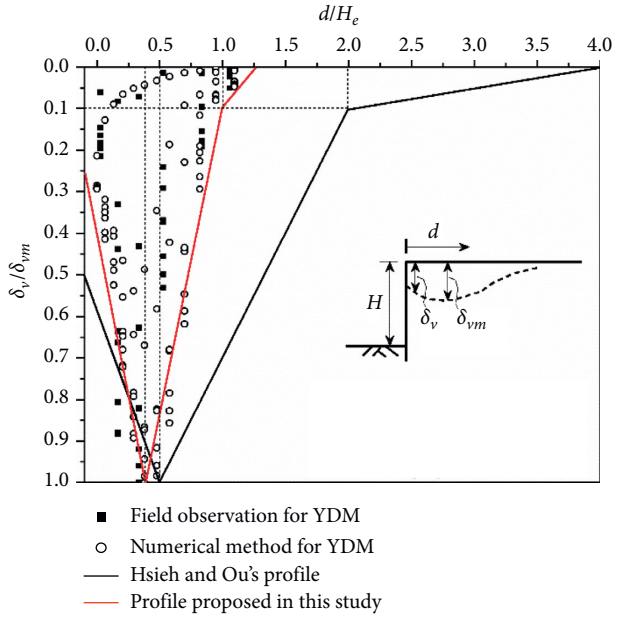

Figure 8: The surface settlement profile for YDM project and Hsieh [28].

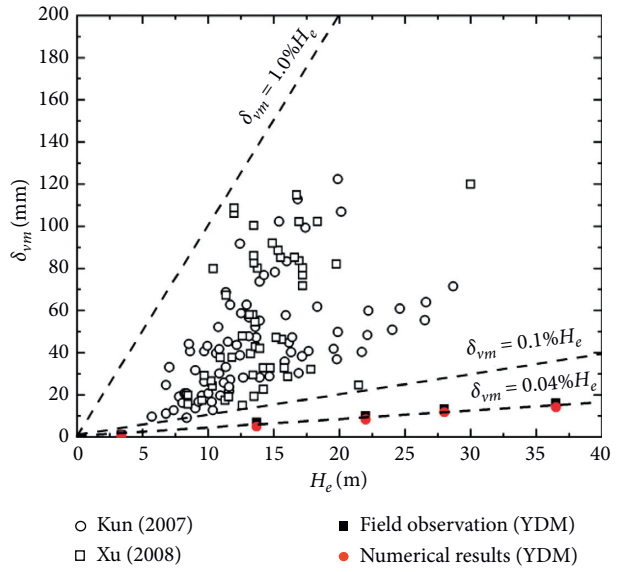

Figure 9: He versus δ_{vm} for YDM project and other dates.

Similar to the surface settlement, most of the deformation occurred between step 1 and step 4. The maximum δ_h of 3D-analysis and observations reached 16.1 mm and 19.1 mm in step 4, which had already accounted for 96.4% and 97.4% of the final deformation (16.7 mm and 19.6 mm), respectively. During the underwater excavation (step 6), the maximum δ_h of 3D-analysis and observation were increased by 1.2 mm and 1.3 mm, which only accounted for 7.2% and 6.6% of the final deformation. Besides, δ_h had a certain reduction during the water recharge (step 5) and bottom sealing (step 7). Therefore, adopting the measures of water recharge and bottom sealing in time was necessary to resist wall deformation during underwater excavation.

Figures 12 and 13 show the relationship between the maximum wall deformation (δ_{hm}) and maximum deformation position ($H_{\delta m}$) with the relation between the excavation depth (H_e). Owing to the underwater excavation methods and the installation of cross walls, δ_{hm} of the YDM project was about 0.06% H_e. This value was far less than the statistical results by Ou [31] and Kung [29], which showed δ_{hm} were nearly 0.2% He or 0.5% He , respectively. Ou [31] concluded that the position of δ_{hm} was located approximately near the excavation surface and was basically within the range of $H_e - 5\text{m} \sim H_e + 5\text{m}$. Nevertheless, the corresponding relationship was $H_{\delta m} = 0.5H_e$ in YDM project. It proved that the location of maximum lateral deflection does

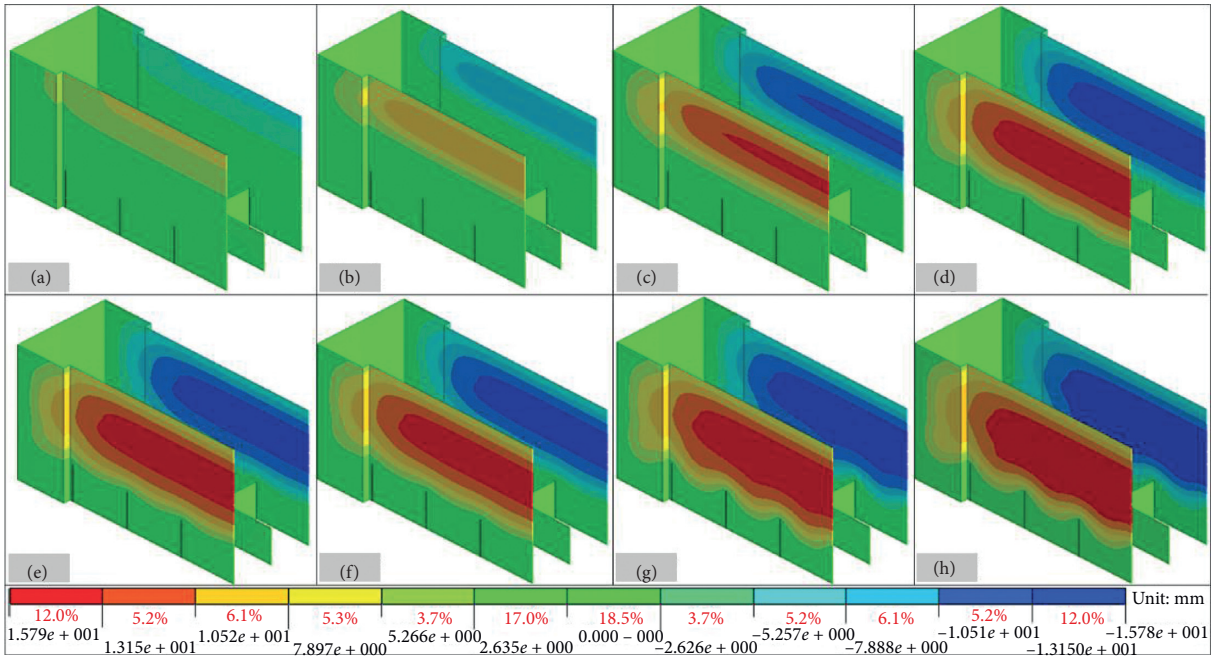

Figure 10: The contour of the lateral wall deflection with 3D-analysis. (a) Step 1, (b) step 2, (c) step 3, (d) step 4, (e) step 5, (f) step 6, (g) step 7, and (h) step 8.

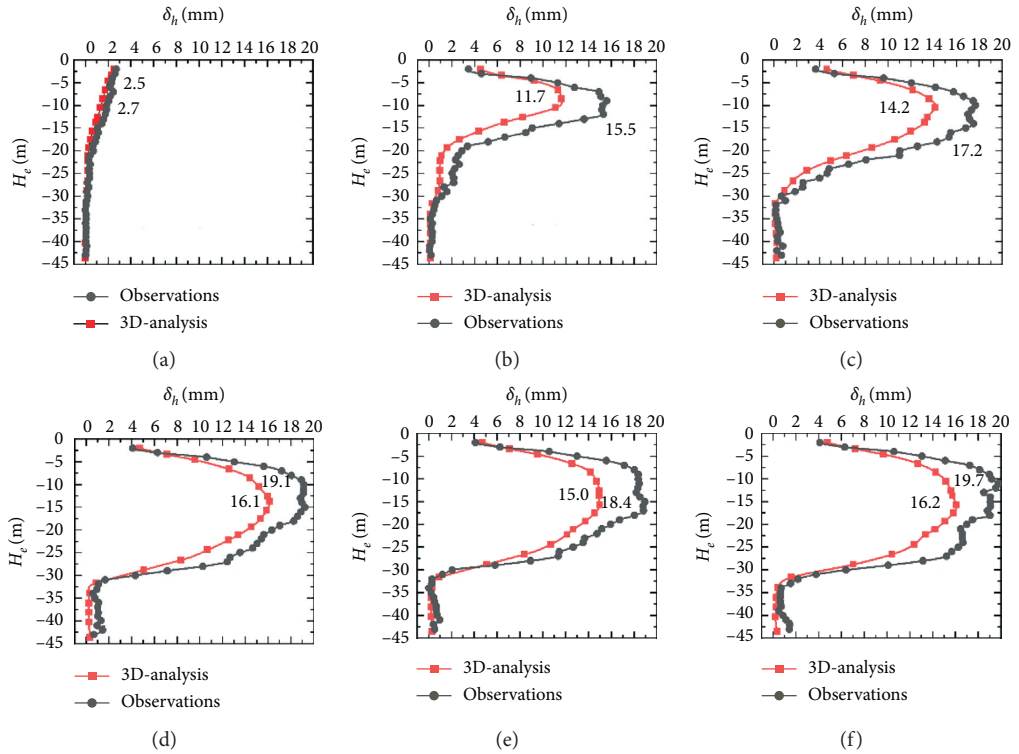

Figure 11: Continued.

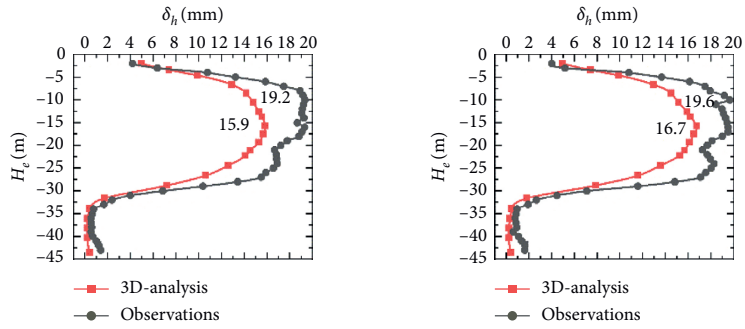

Figure 11: Lateral wall deflection curve under various working conditions for YDM project. (a) Step 1, (b) step 2, (c) step 3, (d) step 4, (e) step 5, (f) step 6, (g) step 7, and (h) step 8.

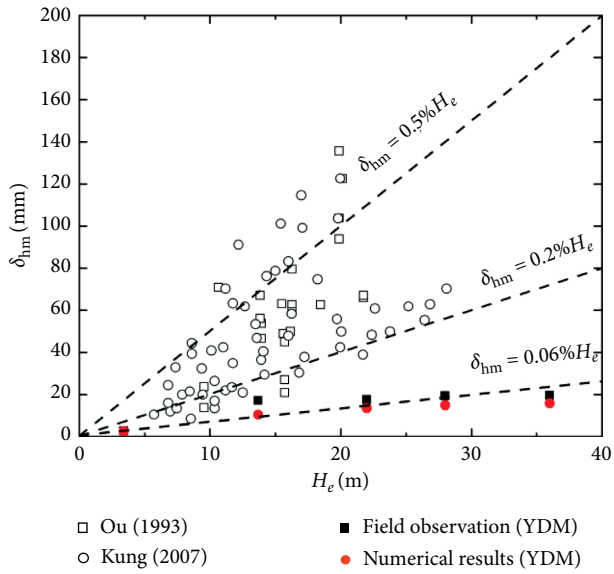

Figure 12: He versus δ_{hm} for YDM and other dates.

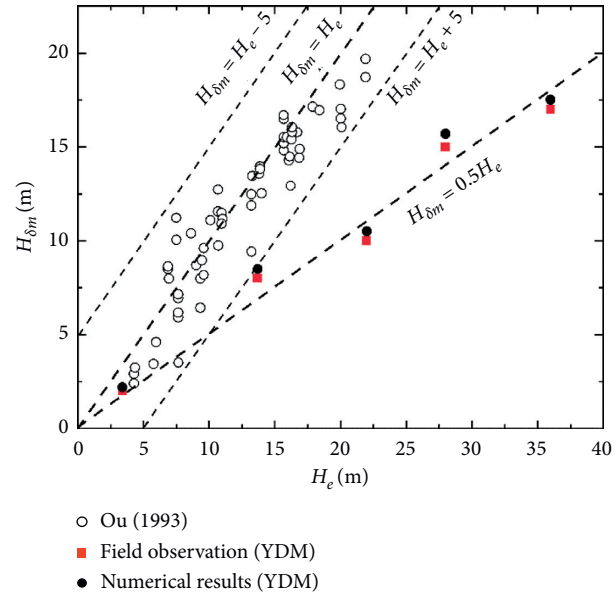

Figure 13: He versus $H_{\delta m}$ for YDM t and Ou [31].

not continue to move down with the increase of excavation depth during the underwater excavation stage which has a positive effect on ensuring the deep stability of the excavation.

This phenomenon could be explained as follows. During the underwater excavation stage, the water pressure can resist part of Earth pressure, and the stress release speed of the diaphragm wall was far less than that of the dry excavation. Besides, the lateral wall deflection was limited when it extends to the position of the cross wall, for which the resistance effect was much better than the upper support.

4. Parametric Study on Underwater Excavation

4.1. Water Recharge. To illustrate the effect of water recharge during the underwater excavation, the final wall deformation with water recharge and without water recharge is as shown in Figure 14. In the recharge area (GL-19 m ~ GL36 m), δ_h increased rapidly below the water level and $H_{\delta m}$ moved to the excavation bottom without water recharge condition. Compared with the water recharge excavation, δ_{hm} reached 36.1 mm and increased by 58%, which was far beyond the deformation limit in the specification. Furthermore, δ_h without water recharge decreased rapidly near the cross wall, but there was still a deformation of 5 mm at the feet of the diaphragm wall.

It indicated that, under the condition of dewatering excavation (without water recharge), the water head difference on both sides of the wall increased with the Earth excavation, which results in large water and Earth pressure acting on the diaphragm wall. Moreover, seepage action occurred at the corner of the wall due to the strong permeability of the pebble layer, which will lead to an inclined failure of the diaphragm wall. Therefore, recharging the water level in time and keeping equal water head on both

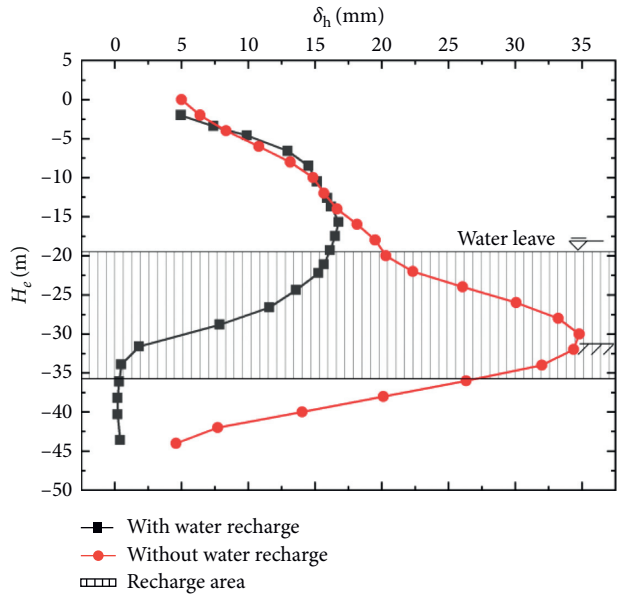

FIGURE 14: δ_h versus H_e for water recharge and without water recharge.

sides of the wall was a key step in underwater excavation to reduce wall deformation.

4.2. Insertion Ratio of Diaphragm Wall. The diaphragm-cross wall system was the retaining structures to ensure the implementation of the underwater excavation. Figure 15 shows the optimization target parameters of retaining wall structure.

The insertion ratio of the diaphragm wall was the ratio of the embedded depth of the diaphragm wall (H_{dw}) to the final excavation depth (H_e), as shown in Figure 15(a). Keeping other parameters of the model unchanged, the insertion ratio of the diaphragm wall was adjusted to 0.07, 0.14, 0.21, 0.28, and 0.35, respectively, and lateral wall deflection was made as in Figure 16.

The deformation curve was basically coincident when the insertion ratio was 0.14, 0.21, 0.28, and 0.35, but increased at the insertion ratio of 0.07. The deformation decreased with the increase of the insertion ratio until it reached a limit value of 0.14 in the YDM project. Furthermore, the deformation still maintained a small value even when the insertion ratio was 0.07. Therefore, with the underwater excavation method, the embedded depth of the diaphragm wall can be appropriately reduced to speed up the construction progress and save the cost.

4.3. Embedded Ratio of the Cross Wall. Theoretically, the deflection of the diaphragm wall was the smallest at the time of $(h_{cw}/h_{dw}) = 1$, but it wasted construction costs. Therefore, a critical embedded depth ratio $(h_{cw}/h_{dw})_{cr}$ was defined to study the optimal cross wall embedded ratio. Any value beyond this critical ratio would no longer cause the deflection value to decrease.

By plotting the relationship between the maximum lateral deflection ($\delta_{h\,max}$) and the ratio of (h_{cw}/h_{dw}), the critical embedding depth for this project can be expressed as $(h_{cw}/h_{dw})_{cr} = 0.5$, as shown in Figure 17. When $(h_{cw}/h_{dw})_{cr}$ was less than 0.5, the value of $\delta_{h\,max}$ decreased as the ratio increased; when $(h_{cw}/h_{dw})_{cr}$ was greater than 0.5, the value of $\delta_{h\,max}$ remained unchanged. This meant that if the project did not take into account other construction factors such as concrete filling, it was most reasonable to set the embedded depth of the cross wall as half of the embedded depth of the diaphragm.

4.4. Interval of the Cross Wall. For the specified excavation size, the ratio of the excavation width B to the cross wall interval L can be used to study the cross wall interval. Figure 18 shows the lateral wall deflection at different values of $(B/L) = 4, 6, 8, 16$.

The deformation trend of the four curves began to differentiate below GL-15 m which meant that the influence range of the cross wall on the lateral wall deflection was below −15 m in the YDM project. Comparing the layout $(B/L) = 16$ with $(B/L) = 8$, although the number of cross walls had doubled, the influence on the lateral wall deflection was only about 0.5 mm difference between GL-20 m and GL-30 m. The displacement of the lower part of the diaphragm wall increased obviously after decreasing the value of $(B/L) = 6$ and $(B/L) = 4$, which was not conducive to the stability of the structure in the range of GL-25 m and GL-40 m. Consequently, the layout with $(B/L) = 8$ considered both the economy and safety of the YDM project.

4.5. Layout of the Cross Wall. Under the condition that the number of the bays was determined, the arrangement forms of 8 vertical bays and 8 horizontal bays are designed to study the effect of the layout of the cross wall (Figure 15(b)). Figures 19 and 20 plot the wall displacement cloud chart and

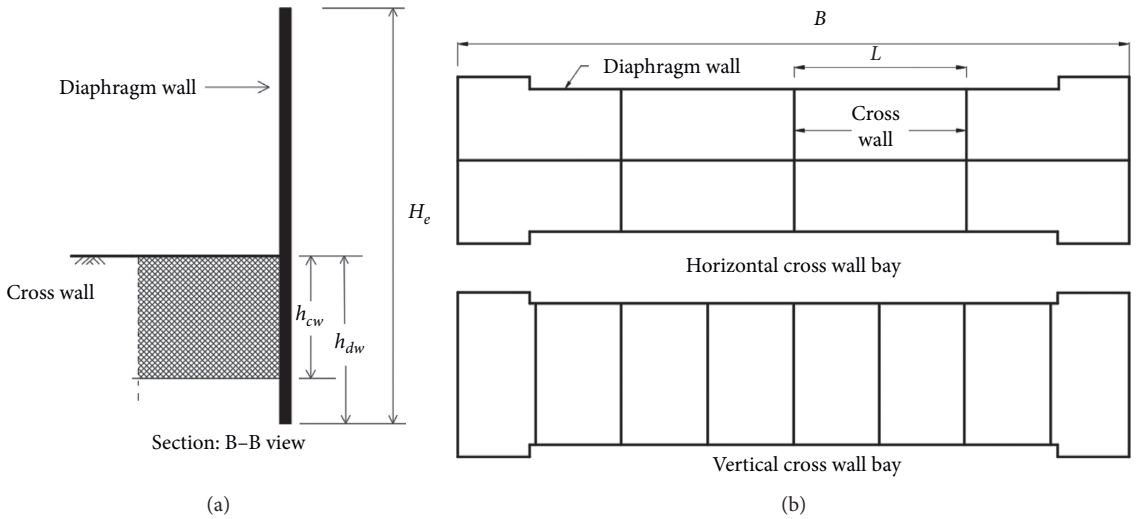

Figure 15: Schematic diagram of the target optimization parameters for retaining. (a) Embedded depth of walls. (b) Geometric parameters of the cross wall.

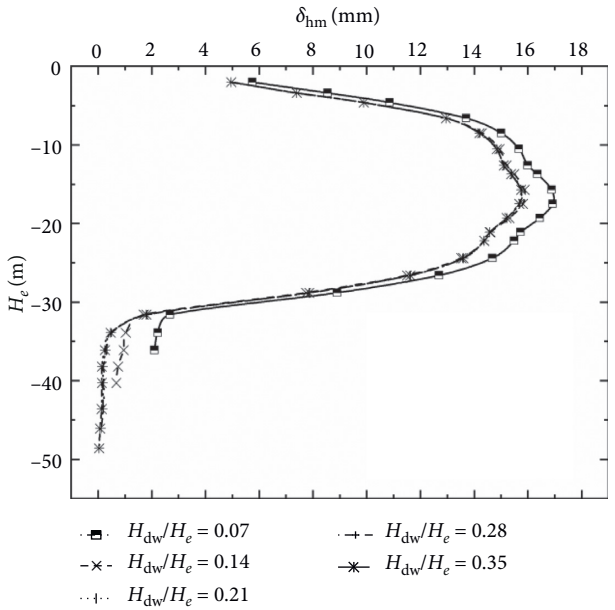

Figure 16: Deflection of diaphragm wall under different insertion ratio.

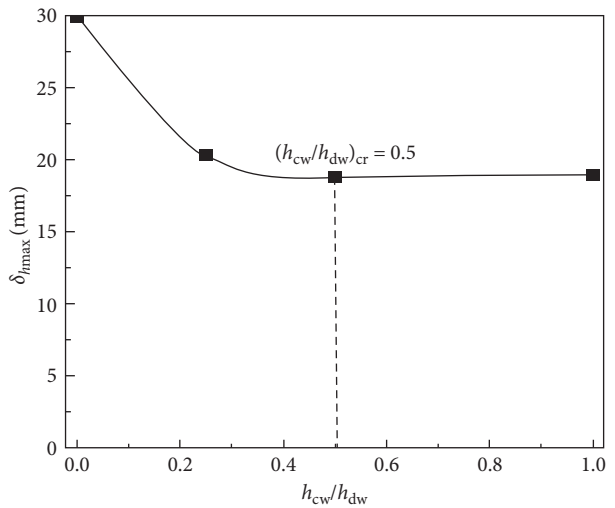

Figure 17: Relationship between $\delta_{h\max}$ and (h_{cw}/h_{dw}).

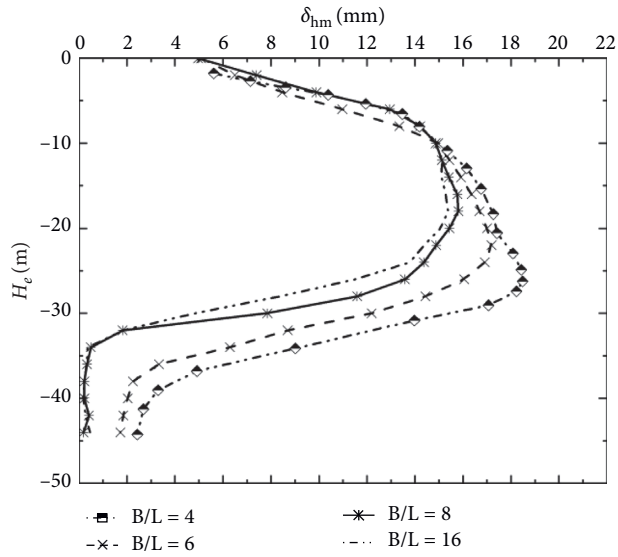

Figure 18: Deflection of diaphragm wall under the different value of (B/L).

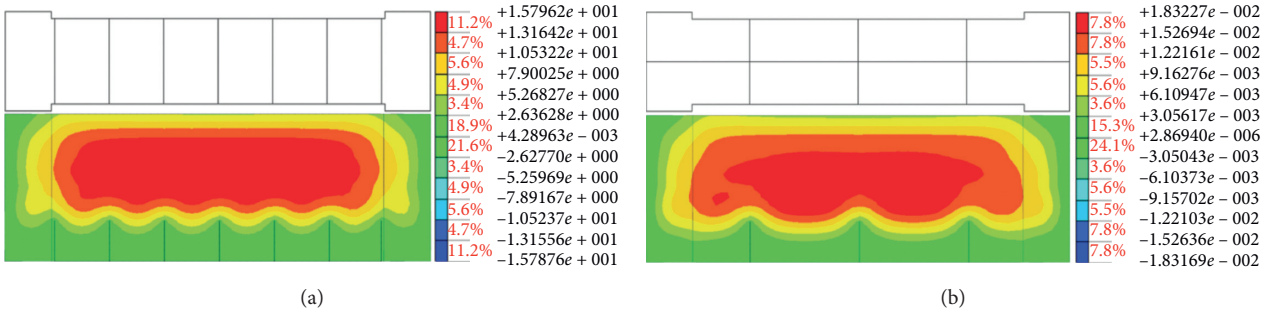

Figure 19: Wall deflection under two different layout forms of the cross wall. (a) Vertical cross wall bay. (b) Horizontal cross wall bay.

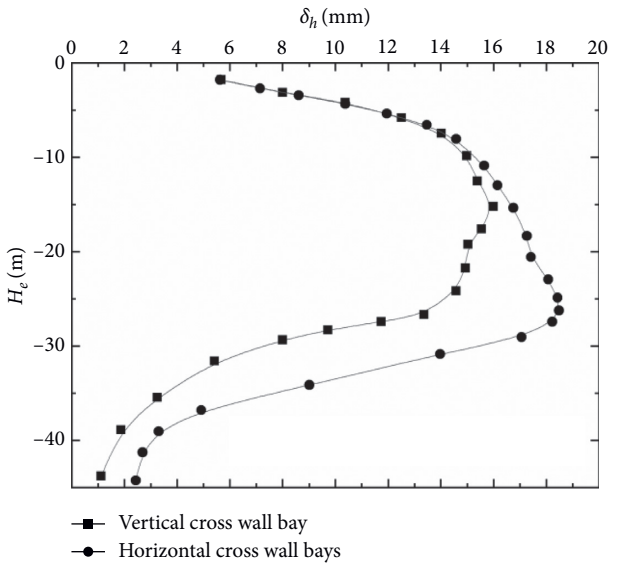

Figure 20: The wall deflection under two different layouts of the cross wall.

the deflection at the midline of the long side of the diaphragm wall in the two different cases, respectively.

Figure 19 plots the increase of the deflection occurring mainly between two cross walls after the excavation was near the cross wall. The wall deformation of the lower part was larger and it developed deeper to the bottom under the condition of the horizontal layout of 8 bays. At the depth of −26 m, the maximum displacement under the vertical layout of the cross wall bay was 11.50 mm, which had a reduction of 37% compared with the wall deflection under the horizontal bays at the same location that was 18.25 mm, as shown in Figure 20. Therefore, the vertical cross wall bays had a better counteraction on the lateral deformation. While ensuring the convenience of concrete casting and underwater excavation, the cross wall can be reduced appropriately. However, the most reasonable way to reduce the cross wall was to minimize the cross wall parallel to the long side of the diaphragm wall and to ensure the cross wall perpendicular to the diaphragm wall. When choosing the same space area, it was better to use vertical cross wall bays.

5. Conclusions

Based on field observations and 3D-analysis results of the YDM project with the underwater excavation method, the deformation behavior of the surface settlement and the lateral wall deflection were conducted. The main findings and conclusions of this study were summarized as follows:

(1) By the hardening soil model, a 3D numerical analysis method for the underwater excavation model was established to analyze the surface settlement and the lateral wall deflection.

(2) Most surface settlements mainly occurred in the stage of dry excavation and dewatering excavation, and the deflection caused by underwater excavation only accounted for about 10% of the total settlement. Meanwhile, the influence range of settlement was approximately equal to the excavation depth. The maximum value of settlement occurred 0.25~0.5 H_e behind the retaining wall and the maximum value was basically 0.04% H_e, which was much less than the predicted value under other dewatering excavations.

(3) Most of the lateral wall deflection has been caused before the underwater excavation, and the deflection only accounted for about 7% of the total deflection in the underwater excavation stage. The maximum wall deflection was about 0.06% H_e, which was far less than the deflection statistics of other similar excavations. Besides, the location of the maximum wall deflection was half of the excavation depth (0.5 H_e).

(4) A novel retaining wall structure based on the underwater excavation method was optimized, and the wall deformation was suppressed with a much smaller embedded ratio of 0.07. In fact, setting the critical interval ratio of the cross wall, $(B/L)_{cr} = 8$, the critical embedded depth ratio of the cross wall, $(h_{cw}/h_{dw})_{cr} = 0.5$, and using the vertical cross wall bays were more advantageous to controlling wall deformation.

Abbreviations

H_e: Excavation depth, m
h_w: Embedding depth of diaphragm wall, m
h_{cw}: Embedding depth of cross wall, m
B: Excavation width
δ_v: Ground surface subsidence, mm
δ_{vm}: Maximum ground surface subsidence, mm
δ_h: Lateral wall deflection, mm
δ_{hm}: Maximum lateral wall deflection, mm
ψ: The angle of dilatancy
E_{50}^{ref}: Modulus of elasticity under partial loading, MPa
E_{oed}^{ref}: Modulus of elasticity of de in compression test, MPa
E_{ur}^{ref}: The referential unloading/reloading stiffness, MPa
m: Power index of the stress level of stiffness
R_f: Poisson's ratio in the unloading-reloading state
v_{ur}: Pore-throat ratio
K_0^{NC}: K_0 value for normal consolidation
d: Horizontal distance to the diaphragm wall, m
t_w: Thickness of the diaphragm wall, m
t_{cw}: Thickness of the cross wall, m
L: Interval of the cross wall, m
c: Cohesion, kPa
φ: Internal friction angle, °
e: Void ratio
C_s: Swelling index.

Data Availability

The data used to support the findings of this study are available from the corresponding author upon request.

Conflicts of Interest

The authors declare that they have no conflicts of interest.

Acknowledgments

This research was financially supported by the Ministry of Housing and Urban-Rural Development of the People's Republic of China with Grant No. 2016-K4-056.

References

[1] E. H. Y. Leung and C. W. W. Ng, "Wall and ground movements associated with deep excavations supported by cast in situ wall in mixed ground conditions," *Journal of Geotechnical and Geoenvironmental Engineering*, vol. 133, no. 2, pp. 129–143, 2007.

[2] T. D. Rourke, "Ground movements caused by braced excavations," *Journal of the Geotechnical Engineering Division, ASCE*, vol. 107, no. 9, pp. 1159–1178, 1981.

[3] X. L. Yang and W. T. Li, "Reliability analysis of shallow tunnel with surface settlement," *Geomechanics and Engineering*, vol. 12, no. 2, pp. 313–326, 2017.

[4] K. S. Wong, I. H. Wong, and B. B. Broms, "Methods of improving the stability of deep excavations in soft clay," in *Proceedings of the 8th Asian Regional Conference on Soil Mechanics and Foundation Engineering*, Kyoto, Japan, July 1987.

[5] G. B. Liu, C. W. Ng, and Z. W. Wang, "Observed performance of a deep multistrutted excavation in Shanghai soft clays," *Journal of Geotechnical and Geoenvironmental Engineering*, vol. 131, no. 8, pp. 1004–1013, 2005.

[6] Y. P. Tan, J. J. Chen, and J. H. Wang, "Practical investigation into two types of analyses in predicting ground displacements due to dewatering and excavation," *Journal of Aerospace Engineering*, vol. 28, no. 6, Article ID A4014001, 2014.

[7] E. Pujades, E. Vázquez-Suñé, J. Carrera et al., "Deep enclosures versus pumping to reduce settlements during shaft excavations," *Engineering Geology*, vol. 169, pp. 100–111, 2014.

[8] Y. Q. De SimoneVilarrasa, J. H. Wang, and M. G. Li, "Effect of dewatering in a confined aquifer on ground settlement in deep excavations," *International Journal of Geomechanics*, vol. 18, no. 10, pp. 04018120.1–04018120.13, 2018.

[9] N. Miyake, N. Kohsaka, and A. Ishikawa, "Multi-aquifer pumping test to determine cutoff wall length for groundwater flow control during site excavation in Tokyo, Japan," *Hydrogeology Journal*, vol. 16, no. 5, pp. 995–1001, 2008.

[10] J. Wang, L. Hu, L. Wu, Y. Tang, Y. Zhu, and P. Yang, "Hydraulic barrier function of the underground continuous concrete wall in the pit of subway station and its optimization," *Environmental Geology*, vol. 57, no. 2, pp. 447–453, 2009.

[11] Y. X. Yang, S. L. Shen, Y. S. Xu, and Z. Y. Yin, "Characteristics of groundwater seepage with cut-off wall in gravel aquifer. I: field observations 1," *Canadian Geotechnical Journal*, vol. 52, no. 10, Article ID 150223161106004, 2015.

[12] H.-S. Hsieh, C.-C. Wang, and C.-Y. Ou, "Use of jet grouting to limit diaphragm wall displacement of a deep excavation," *Journal of Geotechnical and Geoenvironmental Engineering*, vol. 129, no. 2, pp. 146–157, 2003.

[13] L. J. Almaleh, J. D. Grob, and R. H. Gorny, "Ground stabilization for foundation and excavation construction in Florida karst topography," *Environmental Geology*, vol. 22, no. 4, pp. 308–313, 1993.

[14] A. Archontidou-Argyri, A. Simossi, and J. Y. Empereur, "The underwater excavation at the ancient port of Thasos, Greece," *International Journal of Nautical Archaeology*, vol. 18, no. 1, pp. 51–59, 2007.

[15] Y. H. Hu, "Analysis and countermeasures of anti-gushing in excavation of Linjiang super-deep foundation pit with high confined water: taking Meizizhou wind shaft foundation pit of Weisan Yangtze river tunnel in Nanjing as an example," *Tunnel Construction (Chinese and English)*, vol. 35, no. 11, pp. 1194–1201, 2015.

[16] C. S. Qu and D. Xu, "Application of groundwater recharge in dewatering of foundation pit near metro," *Geotechnical Engineering Technology*, vol. 26, no. 5, pp. 238–241, 2012.

[17] C. Jiang, J.-L. He, L. Liu, and B.-W. Sun, "Effect of loading direction and slope on laterally loaded pile in sloping ground," *Advances in Civil Engineering*, vol. 2018, no. 4, 12 pages, Article ID 7569578, 2018.

[18] Y. Sun and H.-S. Yu, "A kinematic hardening soil model considering the principal stress rotation," *International Journal for Numerical and Analytical Methods in Geomechanics*, vol. 37, no. 13, pp. 2106–2134, 2013.

[19] M. D. Bolton, "The strength and dilatancy of sands," *Géotechnique*, vol. 36, no. 1, pp. 65–78, 1986.

[20] M. Calvello and R. J. Finno, "Selecting parameters to optimize in model calibration by inverse analysis," *Computers and Geotechnics*, vol. 31, no. 5, pp. 410–424, 2004.

[21] M. Khoiri and C. Y. Ou, "Evaluation of deformation parameter for deep excavation in sand through case histories," *Computers and Geotechnics*, vol. 47, no. 1, pp. 57–67, 2004.

[22] A. Lim, C. Y. Ou, and P. G. Hsieh, "Evaluation of clay constitutive models for analysis of deep excavation under undrained conditions," *Journal of Geoengineering*, vol. 5, no. 1, pp. 9–20, 2010.

[23] T. Schanz, P. A. Vermeer, and P. G. Bonnier, "The hardening soil model formulation and verification," in *Beyond 2000 in Computational Geotechnics*, R. B. J. Brinkgreve, Ed., Balkema, Rotterdam, Netherlands, pp. 281–296, 2019.

[24] J. M. Duncan and C. Y. Chang, "Nonlinear analysis of stress and strain in soils," *Journal of the Soil Mechanics and Foundations Division*, vol. 96, no. 5, pp. 637–659, 1970.

[25] J. Jaky, "The coefficient of earth pressure at rest," *J Soc Hung Archit Eng*, vol. 78, no. 22, pp. 355–358, 1994.

[26] S. H. Chen, G. J. Wang, H. Zhou, W. M. Wang, and L. C. Zou, "Evaluation of excavation-induced relaxation and its application to an arch dam foundation," *International Journal for Numerical and Analytical Methods in Geomechanics*, vol. 36, no. 2, pp. 166–181, 2012.

[27] F. Dengg, O. Zeman, K. Voit, and K. Bergmeister, "Fastening application in concrete using recycled tunnel excavation material," *Structural Concrete*, vol. 19, no. 2, pp. 374–386, 2018.

[28] P.-G. Hsieh and C.-Y. Ou, "Shape of ground surface settlement profiles caused by excavation," *Canadian Geotechnical Journal*, vol. 35, no. 6, pp. 1004–1017, 1998.

[29] G. T. Kung, C. H. Juang, E. C. Hsiao, and Y. M. Hashash, "Simplified model for wall deflection and ground-surface settlement caused by braced excavation in clays," *Journal of Geotechnical and Geoenvironmental Engineering*, vol. 133, no. 6, pp. 731–747, 2007.

[30] Z. H. Xu, J. H. Wang, and W. D. Wang, "Deformation behavior of diaphragm walls in deep excavations in Shanghai," *China Civil Engineering Journal*, vol. 41, no. 8, pp. 81–86, 2008.

[31] C.-Y. Ou, P.-G. Hsieh, and D.-C. Chiou, "Characteristics of ground surface settlement during excavation," *Canadian Geotechnical Journal*, vol. 30, no. 5, pp. 758–767, 1993.